Powder Technology 283 (2015) 462–474

Contents lists available at ScienceDirect

Powder Technology

journal homepage: www.elsevier.com/locate/powtec

A micromechanical study on the stress rotation in granular materials due to fabric evolution

Ehsan Seyedi Hosseininia *

Civil Engineering Department, Faculty of Engineering, Ferdowsi University of Mashhad, P.O. Box 91775-1111, Mashhad, Iran

ARTICLE INFO

Article history:
Received 21 May 2014
Received in revised form 26 May 2015
Accepted 4 June 2015
Available online 10 June 2015

Keywords:
Anisotropy
Fabric
Non-coaxiality
DEM simulation
Micromechanics

ABSTRACT

In the present study, the non-coaxiality between the axes of principal stress and strain rate tensors is investigated from micromechanical point of view. Based on the so called stress–force–fabric (SFF) relationship, which describes the macro–micro relation, an expression is derived for the principal direction of stress tensor in terms of micromechanical parameters of the fabric. In general, the rotation of principal stress axis and accordingly, the non-coaxiality angle, are influenced by both the anisotropy coefficients and directions of anisotropy of the fabric characteristics. The derived macro–micro relationship was evaluated by performing DEM simulations of 2D specimens of aggregates. It was shown that the principal directions of anisotropy parameters are almost coincident for the assemblies containing circular particles or elongated angular particles with random distribution. In such case, the principal direction of stress tensor can be regarded as the average principal direction of anisotropy. However, when the aggregate with elongated particles has inherently-anisotropic fabric, a correct estimation of the stress angle rotation requires considering all the anisotropy parameters including both anisotropy coefficients and directions.

1. Introduction

In the practical and conventional soil elastic–plastic constitutive models, it is generally assumed that the principal axis of stress coincides with that of the strain rate, i.e., the principle of coaxiality [1]. However, there are experimental and micromechanics-based observations to indicate that these principal axes do not coincide. In the soil mechanics literature, it is appeared that Roscoe et al. [2] was the first who reported the results from simple shear tests on sands concerning non-coaxiality of stress and strain rate tensors. Drescher & de Josselin de Jong [3] reported non-coaxiality in the deformation of an assembly of photoelastic disks in the simulation of two-dimensional granular media. High deviations of the axes were also observed in directional shear cell [e.g., 4,5], hollow cylindrical apparatus [e.g., 6–13] and plain strain (Schneebeli cylinder) tests [14]. In all the experiments, it was found that the deviation is significant at small shear strain, but gradually reduces with the increase in the shear strain and they coincide at large deformations. In addition, a change in loading direction may lead to an abrupt change in the non-coaxiality angle [e.g., 5,9,11,15]. Many attempts have been made to consider non-coaxiality effect in domain of constitutive soil modeling too [e.g., 16–22]. The conceptual reason of non-coaxiality can be explained by studying the micromechanical evolutions in the fabric.

In granular materials, it is obvious that the macroscopically observed behavior is in general a consequence of microstructural response at particle scale. In fact, the mechanical behavior can be well interpreted as a consequence of fabric evolution in the granular medium. The technical term 'fabric' describes spatial arrangement of particles, voids, and associated contacts. Based on experimental [e.g., 23–25] as well as numerical studies [e.g., 26–28], micromechanical investigations reveal that reciprocal mechanisms of generation and collapse of column-like microstructures among particles can explain the shear strength mobilization and deformational behavior of the aggregate media during the loading process. Hence, the deviation in the axes of stress and strain rate tensors can be described by the fabric evolution.

Microstructural evolution in a granular assembly depends on fabric anisotropy, which is distinguished by 'inherent' and 'induced' types. Induced anisotropy occurs during the loading process and shear deformation. However, inherent anisotropy is generally initiated during the deposition of soil particles under gravity so that the long axis of particles tends to align in a specific direction, which is termed as bedding plane. Using the so-called directional shear cell apparatus, Wong & Arthur [5] examined the effect of inherent anisotropy on the coaxiality behavior. They observed coaxiality along the plane of isotropy (the plane normal to the bedding angle), while non-coaxiality was clearly observed along other directions.

Many attempts have been made in order to quantitatively describe the fabric in a granular material. For instance, different forms of the so-called 'fabric tensor', which describes either the distribution of contacts among particles or the orientation of particles, were introduced

* Tel.: +98 51 3880 5111; fax: +98 51 38763303.
E-mail address: eseyedi@um.ac.ir.

http://dx.doi.org/10.1016/j.powtec.2015.06.013
0032-5910/

[23,29–32]. Regarding the estimation of stress state in a granular assembly, Hill [33] defined the average stress tensor in terms of applied forces over a homogeneous granular system [see also 3,32,34,35]. Weber [36] introduced a macroscopic stress tensor, which can be calculated from assembly contact forces and the geometrical arrangement of contacting particles. Based on the Weber's equation, Rothenburg [35] showed that the average stress tensor for an assembly comprising circular particles or spheres has the properties of the stress tensor as used in the continuum mechanics, but is derived from consideration of discrete contact forces, contact geometry and principles of static equilibrium. He developed useful relationships for the assemblies with planar particles (circular disks), which equate the micromechanical parameters to the macroscale stress tensor of the system. By assuming that the distributions of average contact force components and contact normals have the same directions of anisotropy, the so-called stress–force–fabric relationship (SFF) was introduced [37] and its applicability was examined for the assemblies with circular [38], elliptical [39] as well as rigid and breakable polygonal particles [40,41], which were randomly distributed. Note that for the inherently-anisotropic assemblies containing elongated particles, however, this relationship is not applicable since the principal directions of contact force and contact normals among particles are not coincident anymore [28]. Li and Yu [42] explored the mechanism of non-coaxiality from the particle scale. They used directional statistical theory to study the anisotropy in the fabrics and characterized stress direction in terms of direction tensors. More recently, Seyedi Hosseininia [43] has introduced a general form of stress–force–fabric relationship for planar particles with arbitrary angular shape and fabric anisotropy. He generalized the Rothenburg's relationship by consideration of the normal and tangential components of the contact vector lengths with respect to the contact plane of two adjacent contacting particles. The proposed relationships were evaluated by performing numerical simulations of inherently anisotropic assemblies with polygonal elongated particle using Discrete Element Method (DEM).

Since DEM captures more detailed data about the inter-particle features, it has been adopted as a complementary tool to the experimental apparatus by which, the macro- and the micro-mechanical behavior of granular assemblies can be studied. Regarding the examination of coaxiality by DEM, Alonso-Marroquin et al. [44] observed non-coaxiality in a two-dimensional (2D) assembly of randomly distributed convex polygons. Another series of 2D DEM simulations were carried out by Thornton & Zhang [45] to study the shear banding and simple shear non-coaxial flow rules. They have reported a non-coaxial behavior similar to the experimental results of Roscoe et al. [2] and Roscoe [46]. Real tests on sands using a hollow cylinder apparatus [e.g., 9–13,15, 47] also showed that non-coaxiality is dependent on the anisotropy as well as the loading history. By using DEM and considering two-clumped circular disks as one rigid particle, Li and Yu [48] showed that the coaxiality assumption between the internal structure and the contact forces is not valid in the case of non-proportional loading on granular assemblies. They also showed that the simple form of Rothenburg's SSF does not work in such loading condition.

Apart from the particle scale viewpoint, non-coaxiality has been a main issue in constitutive modeling of granular soils from continuum viewpoint. The notion of non-coaxiality is the non-coincidence between principle stress direction and principle plastic strain increment direction. The physical origin of non-coaxial behavior in anisotropic granular media has been clearly identified to be the fabric anisotropy [49,50] and attempts have been made to provide rigorous formulations in the yield surface and flow rules in order to account for fabric effect [e.g., 49, 51–53]. When the formulated model is supplemented by an appropriate micromechanically calibrated fabric evolution law, the non-coaxial behavior in granular media can be convincingly explained and the non-coaxial material response can be predicted.

All the DEM works mentioned above have attempted to relate the existence of non-coaxiality to the anisotropic condition of the fabric in which, the relationship was described qualitatively. The objective of the present study is to investigate more accurately the effect of micromechanical parameters on the deviation of the directions of stress and strain rate axes within a granular material. Based on the generalized form of the micromechanics-based stress–force–fabric relationship [43], a general mathematical expression defining the direction of principal stress axis is derived. Hence, the relationship between fabric parameters and non-coaxiality can be described and discussed quantitatively rather than qualitatively. By using DEM simulations of a granular assembly, the applicability of the expression is examined by fixing the direction of strain rate axis and instead, the deviation of the principal stress axis direction from that of strain rate axis is investigated.

2. Stress–force–fabric relationship

In a granular assembly, the general expression of the Cauchy stress tensor related to microscopic average parameters can be written as follows [43]:

$$\sigma_{ij} = m_v \int_0^{2\pi} \left\{ \overline{f}_n(\theta)\overline{l}_n(\theta)n_i n_j + \overline{f}_n(\theta)\overline{l}_t(\theta)n_i t_j + \overline{f}_t(\theta)\overline{l}_n(\theta)t_i n_j + \overline{f}_t(\theta)\overline{l}_t(\theta)t_i t_j \right\} E(\theta)d\theta. \tag{1}$$

The term m_v is the density of contacts (the number of contacts per unit area). $\vec{n} = (\cos\theta, \sin\theta)$ and $\vec{t} = (-\sin\theta, \cos\theta)$ are the vectors representing the normal and tangential directions with respect to the contact plane between a pair of particles.

In the equation above, $E(\theta)$ indicates the portion of the total number of contacts in the medium, which is oriented at angle θ. The orientation of a contact is defined as the angle between the normal direction to the contact plane and the horizontal direction (see Fig. 1). According to Rothenburg [35], the distribution of contact normal orientation can be approximated by a second-order Fourier series expression:

$$E(\theta) = \frac{1}{2\pi}[1 + a_c \cos 2(\theta - \theta_c)] \tag{2}$$

where a_c describes the anisotropy in contact orientations and θ_c is the major principal direction of anisotropy. The parameter a_c represents the proportional difference in the number of contacts oriented along the major direction of anisotropy, i.e., $\theta = \theta_c$ and that in the perpendicular direction ($\theta = \theta_c \pm 90°$). In other words, if the distribution of

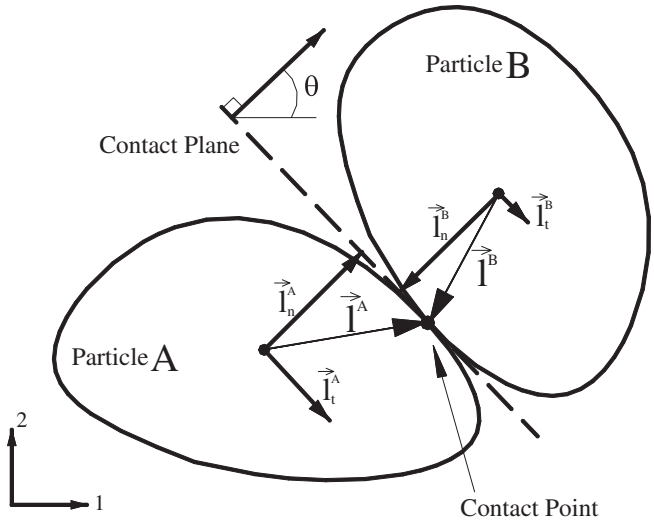

Fig. 1. Schematics of contact vectors and their decomposed components with respect to contact plane for two contacting particles A and B.

normal contacts is sketched in a polar coordinate system named as histogram, a_c is proportional to the difference in the length of the axis along the major principal direction ($\theta = \theta_c$) and the length along the perpendicular direction. If the polar histogram has the form of a circle, the a_c is zero, which corresponds to an isotropic distribution. However, the value of a_c increases and closes to one if the histogram deforms as a peanut, which indicates a high degree of anisotropy condition. The procedure to obtain the anisotropy parameters a_c and θ_c based on the histogram data is explained by Seyedi Hosseininia [28].

The average contact force acting at contacts with an orientation θ is decomposed into the average normal force component $\overline{f}_n(\theta)$ and the average tangential force component $\overline{f}_n(\theta)$. By averaging the contact forces within the group of similar orientation and following the same logic as for contact normals, mathematical expressions for normal and tangential contact forces can be defined as follows [35]:

$$\overline{f}_n(\theta) = \overline{f}_0[1 + a_n \cos 2(\theta - \theta_n)] \tag{3b}$$

$$\overline{f}_t(\theta) = \overline{f}_0[a_w - a_t \sin 2(\theta - \theta_t)] \tag{3c}$$

$\overline{f}_0$ is a constant representing the average normal force over all contacts in the assembly. Similar to θ_c, the terms θ_n and θ_t represent preferred directions of contact force distributions for normal and tangential components, respectively. The terms a_n, a_t and a_w are non-dimensional coefficients of contact force anisotropy. The magnitude of a_n and a_t indicates the differences in average contact forces acting on contacts oriented along the major ($\theta = \theta_n, \theta_t$) and minor ($\theta = \theta_n, \theta_t \pm 90°$) principal stress directions, i.e., perpendicular direction. In contrast to a_c and a_n, the term a_w is not independent and can be defined in terms of a_c and a_t from moment equilibrium of all contacts [43]. Generally, the value of a_w is small and close to zero. Physically, a non-zero value corresponds to a situation where a non-symmetrical distribution of shear contact forces is required to compensate for the lack of contact normals in the direction of loading axis. Values of these parameters can be determined based on regression of histograms data as explained by Seyedi Hosseininia [28].

$\overline{l}_n(\theta)$ and $\overline{l}_t(\theta)$ represent the average length of normal and tangential contact components of the contact vectors acting on the contacts with orientation θ. According to Fig. 1, a pair of particles (A and B) has contacts with corresponding contact vectors $\left(\vec{l}\right)$, which are defined as the vectors connecting from the centroid of the particle to the contact point. $\vec{l}$ is decomposed into normal $\left(\vec{l}_n\right)$ and tangential $\left(\vec{l}_t\right)$ components. The polar distribution of $\overline{l}_n(\theta)$ and $\overline{l}_t(\theta)$ are in the form of Fourier series expressions [43]:

$$\overline{l}_n(\theta) = \overline{l}_0[1 + a_{\ln} \cos 2(\theta - \theta_{\ln})] \tag{4a}$$

$$\overline{l}_t(\theta) = -\overline{l}_0 a_{lt} \sin 2(\theta - \theta_{lt}). \tag{4b}$$

The term $\overline{l}_0$ in the above equations stands for the average length of normal component of contact vectors from all particles in the assembly. The terms $a_{\ln}$ and a_{lt} are non-dimensional coefficients of contact anisotropy, which explain the anisotropic distribution of the normal and tangential components of the contact vectors within the assembly. In an assembly with similar circular particles, we have $a_{\ln} = a_{lt} = 0$, which results in $\overline{l}_n(\theta) = \overline{l}_0$, $\overline{l}_t(\theta) = 0$. In such case, the stress–force fabric relationship (Eq. (1)) gets a simpler form as already described by L. Rothenburg & Selvadurai [37]. A non-zero value for the coefficient a_{lt} represents the deviation of the direction of the contact vector from the contact normal. In an assembly of elongated particles, we might even have $a_{lt} \approx 0$, which means that the elongated particles are isotropically distributed within the assembly. The terms $\theta_{\ln}$ and θ_{lt} represent certain preferred directions of particle contacts. For a general case, where the assembly contains a broad range of sizes of irregular-shaped particles with a random distributions, $\theta_{\ln} \neq \theta_{lt}$, but in the assemblies containing similar particles, these directions are nearly coincident. For instance, the value of these terms for inherently-anisotropic assemblies with the same particle shape is nearly equal to the bedding angle of the particles.

In the derivation of stress tensor governing granular media (Eq. (1)), there is a controversy about its asymmetry. Some researchers claimed that stress tensor is not symmetric in granular media, while others affirm that the stress asymmetry is negligible for practical purposes or its consideration is not necessary in order to avoid complicated descriptions of the mechanical behavior of granular media. Such difference in these two viewpoints originates from the procedure the stress tensor is derived. Bardet and Vardoulakis [54] showed that there is asymmetry in the stress tensor when it is defined from virtual work, but symmetry exists in the tensor when the stress is defined from statics [e.g., 33,35, 36]. They found that the asymmetry originates from external moments, and that the amplitude of stress asymmetry decreases with the size of the granular volume. The stress asymmetry is, therefore, more detectable in elongated samples such as interfaces that are subjected to external moments on their boundary. Bulky samples subjected to small external moments are likely to display negligible stress asymmetry. The stress asymmetry can rightfully be neglected in large masses of granular media far away from the boundaries with external moments. It is also noted here that Eq. (1) is basically derived from statics and thus, the corresponding stress tensor is expected to be symmetric. In Section 4, the symmetry of the stress tensor is investigated by tracing the stress component values.

3. Non-coaxiality angle from macro- and micro-viewpoints

The non-coaxiality angle (ω) is defined as the difference between the principal direction of stress tensor (θ_σ) and that of corresponding incremental strain tensor ($\theta_{\dot{\varepsilon}}$), which means that:

$$\boldsymbol{\omega} = \theta_\sigma - \theta_{\dot{\varepsilon}}. \tag{5}$$

According to loading conditions of a soil element, θ_σ and $\theta_{\dot{\varepsilon}}$ can be fixed or variable. In the current study, the loading condition is defined in such a way that the principal direction of the incremental strain is kept constant, while the principal direction of stress is measured during the loading process (as shown and explained later in Fig. 3). Thus, the macro- and microscopic expressions of θ_σ is introduced in the following subsections.

3.1. Macroscopic expression of θ_σ

According to Fig. 2a, consider a granular assembly whose boundary is applied by stress tensor components σ_{11}, σ_{22}, and $\sigma_{12}(=\sigma_{21})$. The indices correspond to the names of the axes of the coordinate system, where the 1–1 and 2–2 axes are defined in the horizontal and vertical directions, respectively. Hence, σ_{11} and σ_{22} are the horizontal and vertical stress components and σ_{12} and σ_{21} are the tangential (or shear) components applied over the medium boundary.

Based on the continuum mechanics, the principal direction of stress tensor can be obtained by the concept of Mohr's stress circle. As shown in Fig. 2b, the orientation of principal directions of major and minor principal stresses can be determined by measuring the angles $A\hat{O}B$ and $C\hat{O}D$, receptively in the Mohr's circle and taking half of these angles. Thus, the angle between the lines $\overline{OA}$ and $\overline{OB}$ (and similarly between $\overline{OC}$ and $\overline{OD}$) is twice the angle θ_σ known as the principal stress direction. Alternatively, the angle θ_σ can be assessed directly by using trigonometric relationships as follows:

$$\theta_\sigma^{macro} = \frac{1}{2}\tan^{-1}\left(\frac{2\sigma_{12}}{\sigma_{22} - \sigma_{11}}\right). \tag{6}$$

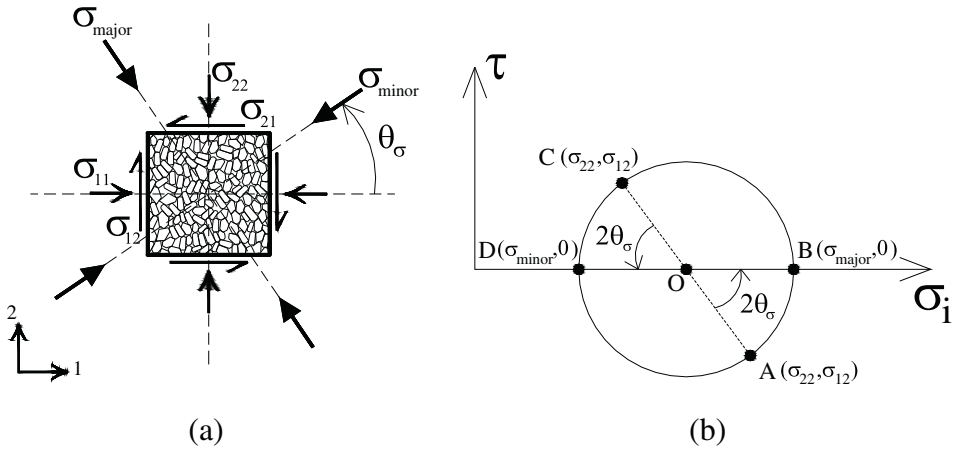

Fig. 2. Macroscopic definition of direction of principal stress axis in (a) granular medium; (b) Mohr's stress circle with respect to applied stress components.

The angle symbol defined above is denoted by the superscript 'macro' since the above relationship is obtained from the macroscopic stress components ($\theta_\sigma = \theta_\sigma^{macro}$).

3.2. Microscopic expression of θ_σ

Following the introduction of the Cauchy stress tensor from micromechanical viewpoint (Eq. (1)), a microscopic expression of the principal stress direction can be obtained. In order to find an expression of θ_σ in terms of micromechanical parameters, it is sufficient to derive the micromechanical expressions of stress components (σ_{ij}, $i, j = 1, 2$) and then substitute them in Eq. (6). After a big amount of integration calculations and mathematical manipulations (see also Appendix A), the following expression can be reached:

$$\theta_\sigma^{micro} = \frac{1}{2}\tan^{-1}\left(\frac{a_c \sin 2\theta_c + a_n \sin 2\theta_n + a_t \sin 2\theta_t + a_{\ln} \sin 2\theta_{\ln} + a_{lt} \sin 2\theta_{lt}}{a_c \cos 2\theta_c + a_n \cos 2\theta_n + a_t \cos 2\theta_t + a_{\ln} \cos 2\theta_{\ln} + a_{lt} \cos 2\theta_{lt}}\right). \tag{7}$$

In the derivation of Eq. (7), the product of anisotropy coefficients for the third and higher orders has been ignored since it is small and insignificant. By this equation, one can thoroughly understand the influencing micromechanical parameters on the rotation of principal stress axis. According to Eq. (7), it is evident that not only the anisotropy directions of contact normals (θ_c), components of force (θ_n, θ_t) and length vectors ($\theta_{\ln}$, θ_{lt}) play role, but also the corresponding coefficients of anisotropy (a_i) can have a great portion of influence on the deviation of principal stress axes. Examination of the above equation can be only possible by using numerical DEM simulations since it requires a detailed trace of micromechanical parameters.

4. Numerical simulations

Numerical simulations are carried out by using Discrete Element Method (DEM). In DEM, a granular medium is considered as a collection of individual rigid particles which can move and rotate due to applied external forces and moments from adjacent particles. DEM is based on dynamics formulations and equations of motion are solved for each particle using implicit time integration method [34]. Time steps are small enough that moderate variation does not significantly influence simulation results. It is noted that in the simulation procedure mentioned in this study, a monotonic loading (in one direction) is only considered; however, the modeling procedure can be upgraded for situations in which, loading direction can be changed. For instance, the samples are loaded reversely along with some cycles or direction of principal stress axes are rotated such that the applied shear stress remains constant during the simulation.

The simulations in the present study concerns 2D biaxial compression tests on aggregates. The samples to be loaded have a form of circle in which the particles are laid down. In the defined monotonic loading, the shearing loading process of the sample is defined by applying controlled displacement condition on the boundaries through the 1–1 and 2–2 axes, as shown in Fig. 3. The sample is assumed to be loaded by boundary particles. In other words, the periphery of the sample is constituted of boundary particles by which, the boundary controlled displacements are applied. In this procedure, the sample, which is already isotropically compressed to a predefined pressure, is loaded by constant incremental displacement in the vertical direction as if two platens in the upper and lower sides of the sample move close to each other. Instead, the lateral sides of the sample move freely in the horizontal direction provided that the pre-defined stress in the horizontal direction (1-axis) remains constant. Over the sample, no incremental shear displacement ($\dot{v} = 0$) is implemented and hence, we have $\dot{\varepsilon}_{ij} = 0$ where $i \neq j$. As a consequence, the direction of principal strain rate axes is fixed and coincides with the global 1–1 and 2–2 axes. In other words, we have: $\theta_{\dot{\varepsilon}} = 90°$. In contrary, since there is no control on the stress components, both normal and shear stress components can be

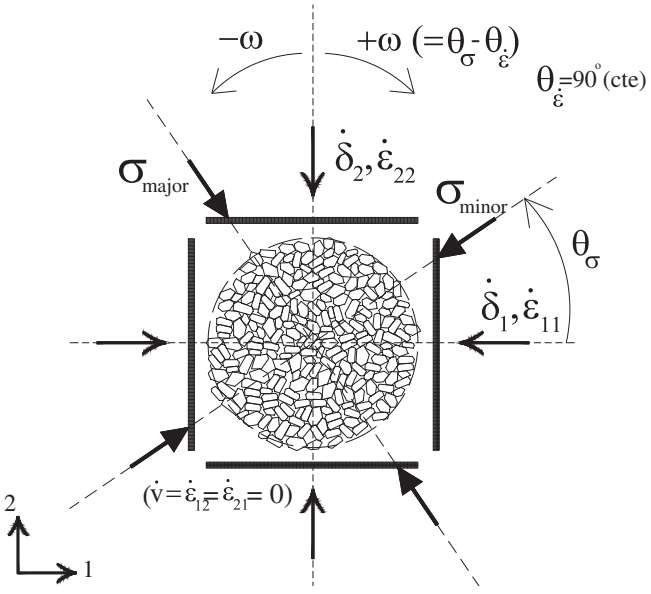

Fig. 3. Definition of boundary conditions in biaxial compression test simulated by DEM and the presentation of non-coaxiality angle (ω) in terms of principal directions of stress (θ_σ) and incremental strain ($\theta_{\dot{\varepsilon}}$).

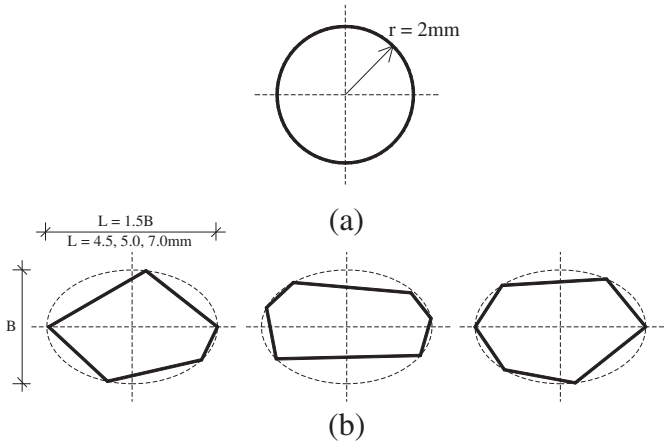

Fig. 4. Geometry and size of the particles used in the simulations: (a) circular particle; (b) elongated polygon-shaped particles.

generated during the loading process. This loading procedure facilitates to investigate the rotation of principal axes of stress in the granular assembly. It is again noted that the principal stress direction is not monotonically rotated, which is quite different from the common term of rotational shear tests in the laboratory. The non-coaxiality angle (ω) can be accordingly obtained for the biaxial samples as follows:

$$\boldsymbol{\omega} = \theta_{\sigma} - \theta_{\dot{\varepsilon}} = \theta_{\sigma} - 90^{\circ}. \tag{8}$$

To micromechanically investigate the fabric evolution of aggregates, two modified versions of DEM-based codes including DISC [55] and POLY [41] have been used for simulations by which, particles can be considered, respectively, as circle and free convex-polygon in shape. A brief review of the numerical procedure used in the simulations can be found in the references Sitharam et al.[56] and Seyedi Hosseininia [27] for circular and polygonal particles, respectively. In what follows,

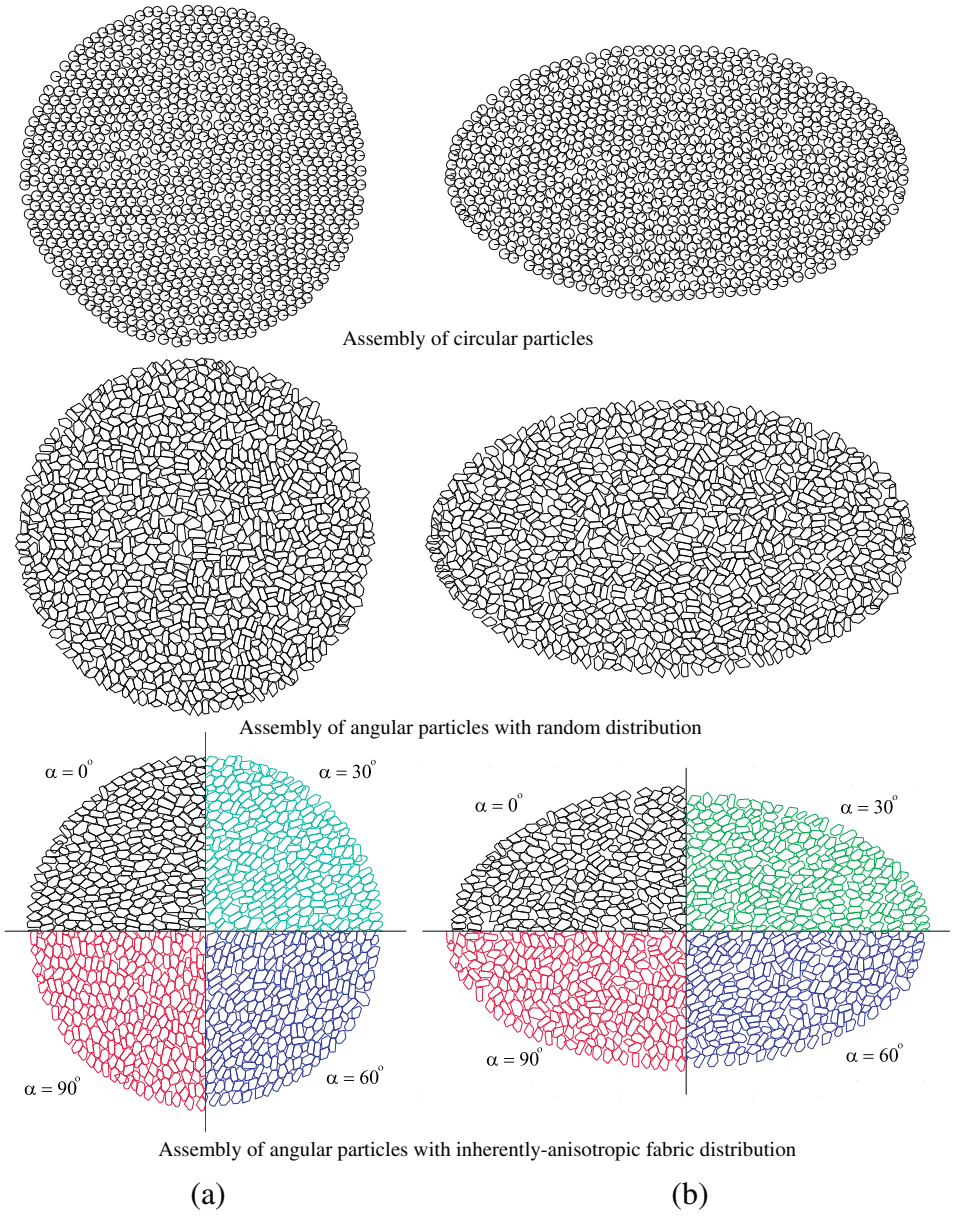

Fig. 5. Schematics of numerical assemblies including circular and elongated angular particles: (a) isotropically-compacted; (b) biaxially-sheared at axial strain of $\varepsilon_{22} = 20\%$.

a brief review of the modeling features of the 2D samples is explained here.

As mentioned before, two types of particle geometry including circular and angular particles are considered in this study. Fig. 4 shows the geometry and sizes of the particles used in the simulations. The circular particle has a radius of 2 mm. The angular particles are elongated and circumscribed by an ellipse with an aspect ratio (length to width axes) of 1.5. For each angular particle, three sizes, represented by the major axis length (L), are considered including $L = 4.5$, 5.0, and 7.0 mm. It is noted that the geometry of angular particles can be arbitrarily defined in the simulations except that the shape should be convex.

In total, six assemblies of aggregates were simulated including one assembly with mono-sized circular particles and five assemblies including a mixture of elongated angular particles. The numerical specimens have a circular form with a diameter of 160 mm in which, about 2000–2500 particles were stacked. Since the diameter of the specimen is large enough with respect to the average particle diameter ($D_{sample}/\overline{D}_{particle} = 30$–$40$), the effect of particle size on test results can be ignored. All the specimens are generated according to the predefined particle size distribution in such a way that the particles are placed in the specimen randomly in condition that they should not be overlapped (see [27] for more information). The assemblies with elongated particles have the same particle frequency distribution, which is characterized by the uniformity coefficient (D_{60}/D_{10}) of 1.35 and the curvature coefficient ($D_{30}^2/D_{10}D_{60}$) of 1.2. D_x indicates the long axis length (diameter of an equivalent circumscribed circle) of the particles for which x% of the particles are finer. Among these assemblies, one assembly contains randomly-oriented distributed particles such that the initial fabric has an isotropic-like condition, while the other four assemblies have been fabricated in such a way that the long axis of all particles be oriented along a pre-defined direction i.e., bedding plane (α). By such arrangements of the particles, these samples have initial anisotropic fabrics. The four initially-anisotropic samples have bedding planes of $\alpha = 0$, 30, 60, and 90° with respect to the horizontal direction.

The loading of each sample is carried out by two stages including a primary compression followed by biaxial shear loading. According to Fig. 5a, all specimens are firstly compressed isotropically under a confining pressure of 300 kPa. The compression process is controlled by radial movement of the boundary particles so that the mean principal stress, i.e., $p = (\sigma_{11} + \sigma_{22})/2$ reaches the defined value (300 kPa). By reaching $p = 300$ kPa, the isotropic loading does not come to end, but it continues until the specimen has no volume change. As the second stage of loading, the specimen is loaded biaxially in such a way that the stress in the lateral direction (1-axis) remains constant and equals $\sigma_{11} = 300$ kPa, while the top and bottom of the specimen are loaded vertically along the 2–2 axis by moving boundary particles with a constant displacement rate proportional to the distance from the center of the specimen. Accordingly, the specimen deforms under such biaxial loading condition and the circular form turns into an elliptical one, which is elongated horizontally (Fig. 5b).

Before starting the main consolidation stage as the first loading stage, an initial compaction of the samples is performed in such a way that the particles get close to each other as much as possible and that no inter-force exists between particles. Indeed, this initial compaction is performed in order to speed and facilitate the process of consolidation stage. This initial stage, which is not included as a part of the consolidation stage, is run by considering zero value for the inter-particle frictional coefficient (μ_s). Afterwards, the main consolidation stage is initiated.

The values of DEM parameters used in the simulations are the same as those mentioned in the reference by Seyedi Hosseininia [27]. The only difference relates to the value of the inter-particle frictional coefficient (μ_s), which is assumed to be constant during both loading stages (consolidation and biaxial shearing) and always equals $\mu_s = 0.5$, while in the previous simulations, μ_s was set to zero for the consolidation stage in order to have the samples with higher compaction. All the samples at the end of the consolidation stage have a dense state (which can be recognized from dilative behavior during shearing) with the void ratio in the range of 0.26–0.28. The void ratios of the anisotropic samples with $\alpha = 0$, 30, 60, and 90° are 0.264, 0.268, 0.272, and 0.263 respectively. The void ratios of the samples with isotropic arrangement of angular particles and circular particles are 0.267 and 0.282, respectively. It is noted that these small values of void ratio only corresponds to 2D samples and the measured void ratios for real sand samples are higher. The

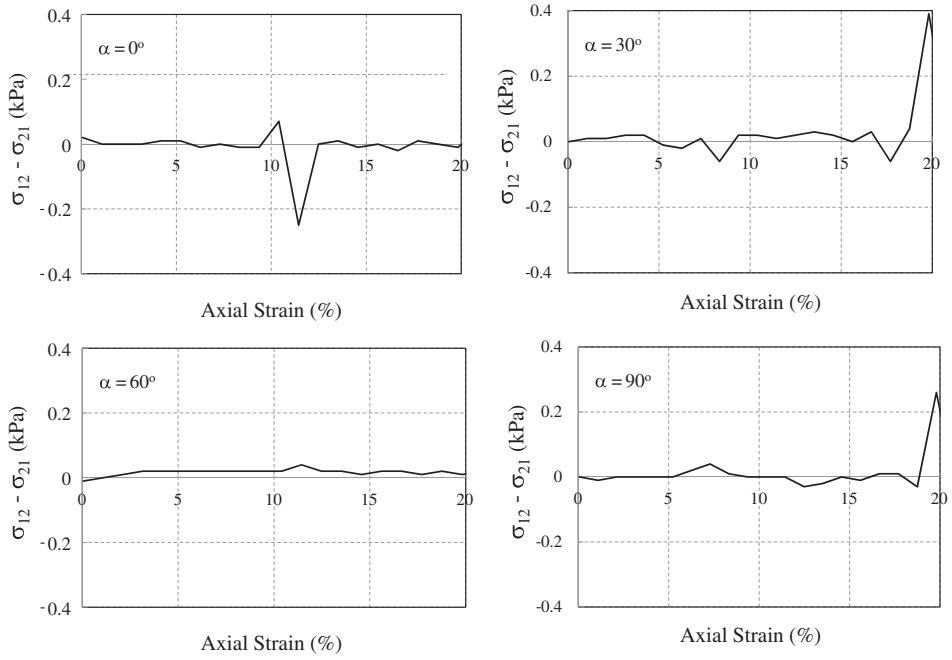

Fig. 6. Evolution of σ_{12}–σ_{21} in the anisotropic assemblies with axial strain.

simulations of biaxial loading stage have been performed until the axial strain of $\varepsilon_{22} = 20\,\%$.

5. Results and discussion

In this section, micromechanical behavior of assemblies is studied, which regards the fabric evolution in terms of variation of micromechanical parameters versus the axial strain during the biaxial loading process. A study on the macroscopic behavior such as shear strength and deformation as well as macro–micro relationships of the macroscopic behavior is out of scope of the present paper. A detailed discussion on these subjects can be found in Seyedi Hosseininia [27,43].

Since the macro- and microscopic formulations of this study are based on the symmetry of the stress tensor, in this part, the symmetry of the Cauchy stress tensor in anisotropic assemblies is investigated. Fig. 6 presents the variation of the difference between diagonal components of stress tensor, $\sigma_{12}-\sigma_{21}$, whose values are calculated directly from Eq. (1). It can be seen that the difference value is very small close to zero that indicates the equality of these stress components and thus the symmetry of the stress tensor.

It is reminded that the general idea of how the microstructure in granular assemblies evolves during the shearing process can be usefully studied by following the change in the number of contacts, the magnitude of average normal and average tangential forces, and the arrangement of particles relative to each other. In this section, the variation of all micromechanical parameters is initially investigated in three categories including the assemblies with circular particles, those with randomly-distributed elongated particles, and inherently-anisotropic assemblies. Then, the magnitudes of the non-coaxiality angle calculated from macro- and micro-relationships are compared with each other.

5.1. Evolution of anisotropy parameters in the fabric

5.1.1. Assembly of mono-sized circular particles

Fig. 7 presents the variation of anisotropy coefficients in the assemblies with circular particles including a_c (contact normals), a_n and a_t (normal and tangential contact forces) and $a_{\ln}$ and a_{lt} (arrangement of particles) as well as their corresponding principal direction of anisotropy along with the axial strain. According to Fig. 7a, the values of a_c, a_n, and a_t parameters increase rapidly from the onset of loading and then, the rate of variations decreases. The parameter a_c, which describes the anisotropy condition in the number of contacts, increases to a peak value along the loading process until the axial strain of about 7% and thereafter, it falls slowly to the end of the test. a_n has the largest value among the parameters accompanying some fluctuations, which can be interpreted as the generation/collapse of force columns in the aggregate [28]. The same description is true for the a_t parameter, but the magnitude is much smaller since the shear stress mobilization is restricted because of slippage phenomenon between particles. The magnitudes of $a_{\ln}$ and a_{lt} are absolutely zero for the whole of the test because of

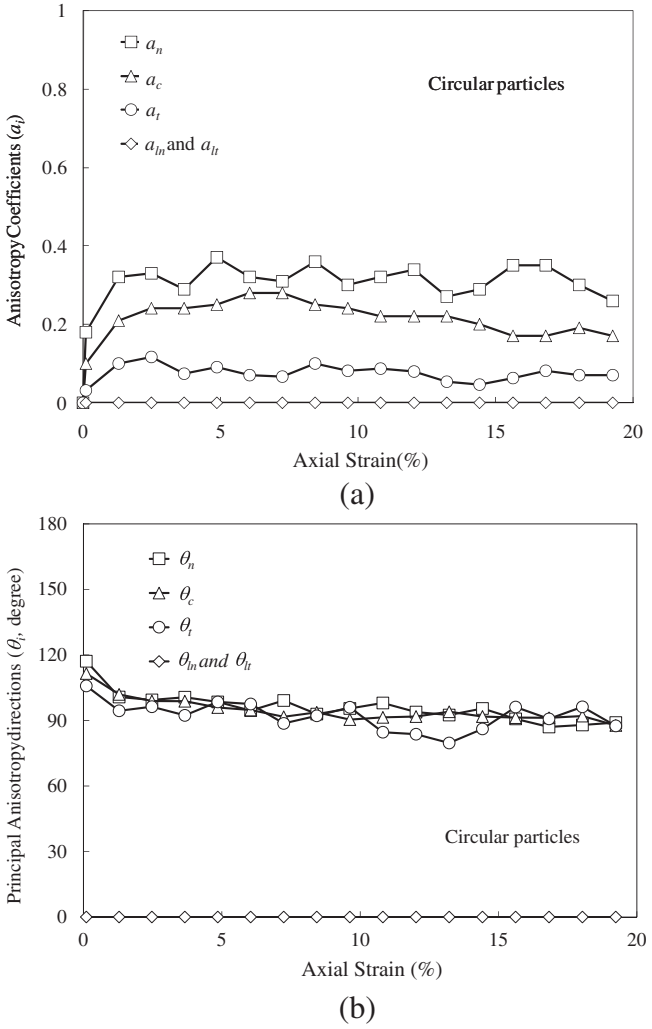

Fig. 7. Variation of (a) anisotropy coefficients and (b) anisotropy principal directions in the assembly with circular particles.

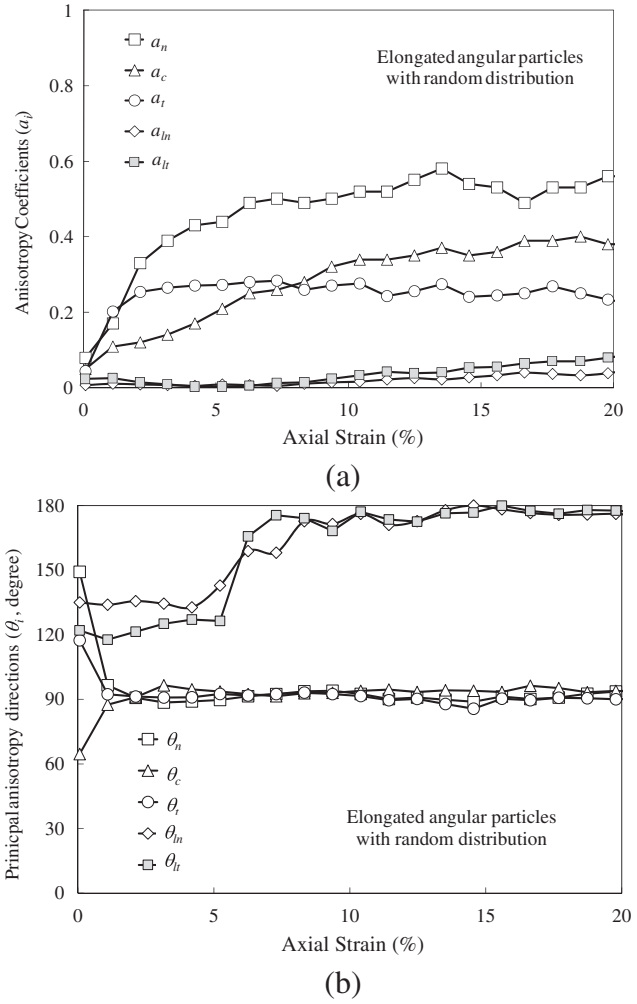

Fig. 8. Variation of (a) anisotropy coefficients and (b) anisotropy principal directions in the assembly of elongated angular particles with random distribution.

the existence of circular particles in the assembly. Referring back to Fig. 1, the contact vector $\left(\vec{l}\right)$ coincides with the normal contact vector $(\vec{l}_n)$ and hence, there is no tangential component $(\vec{l}_t)$ of contacts. In Fig. 7b, the variation of the corresponding principal directions of anisotropy is shown along with the axial strain. With the exception of $a_{\ln}$ and a_{lt} that are zero, the direction of contact normals and normal and tangential contact forces are almost coincident during the test. The initial value starts from about 120° and then it decreases gradually to 90°, which corresponds to the principal direction of strain rate axis.

It is here noted that the obtained results from this 2D simulation are comparable with those of 3D simulations performed by [57]. In their work, a cubic packing of polydisperse spherical particles with radii in the range of 0.2–0.6 mm was considered. In their work, the signature of shear-induced anisotropy in granular media was investigated by tracing the evolutions of different anisotropy components for different initial states under drained/undrained monotonic triaxial compression. By quantitatively comparing the results of these two simulations, it can be seen that similar trends exist for the variation of anisotropic parameters.

5.1.2. Assembly of randomly-distributed angular particles

A trace of the values of micromechanical parameters is shown in Fig. 8 for an assembly containing elongated angular particles. The particles are randomly distributed in such a way that the fabric has an isotropic condition. This can be justified according to Fig. 8a where the initial value of a_i parameters is close to zero. However, by starting the shear loading process, anisotropy induces in the fabric and the a_i parameters begin to grow. The parameter a_n increases rapidly at the initial level of axial strain (until about 5%) followed by a slow grow in magnitude at larger deformation levels. The same initial increase in the mobilization of a_t exists, but after reaching a peak value, it declines gradually as the shear strain continues. This is again related to the shear stress mobilization between particles. The parameter a_c has a continuous growth in value from the beginning to the end of the test, which indicates that the rate of contact generation in the principal direction is higher than that in the perpendicular direction. In comparison with the assembly with circular particles, it can be seen that the magnitude of anisotropic parameters of the assembly with angular particles is bigger than those of the assembly with circular particles. This is owed to the effect of particle geometry. It is known from experimental researches [e.g., 58, 59] as well as numerical studies using DEM [e.g., 41,60–62] that assemblies with sharp edged particles show greater shear strength and dilatancy, due to interlocking effect among particles.

In contrary to the assembly with circular particles, the parameters $a_{\ln}$ and a_{lt} are not zero. The value of these parameters is zero at the beginning, but they grow very slowly to the end of the test by keeping $a_{\mathrm{lt}} > a_{\ln}$. However, the values are still much smaller than other parameters and are close to zero. This is justified by keeping in mind that these parameters represent the average anisotropy condition concerning the

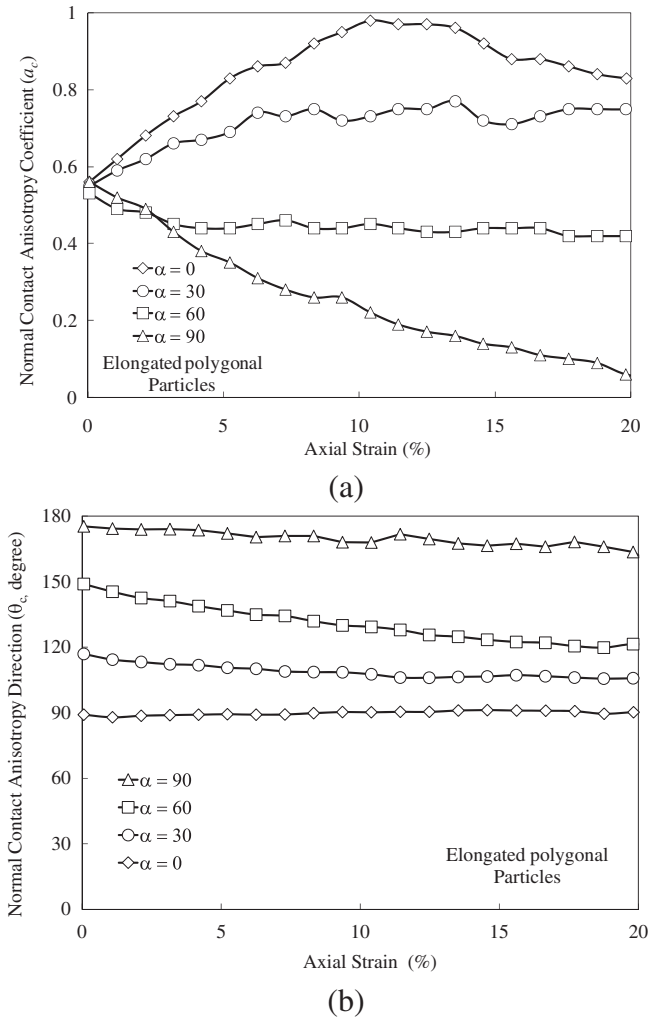

Fig. 9. Variation of contact normal anisotropy parameters versus the axial strain for different bedding angles (a) coefficient of anisotropy; (b) principal direction of anisotropy.

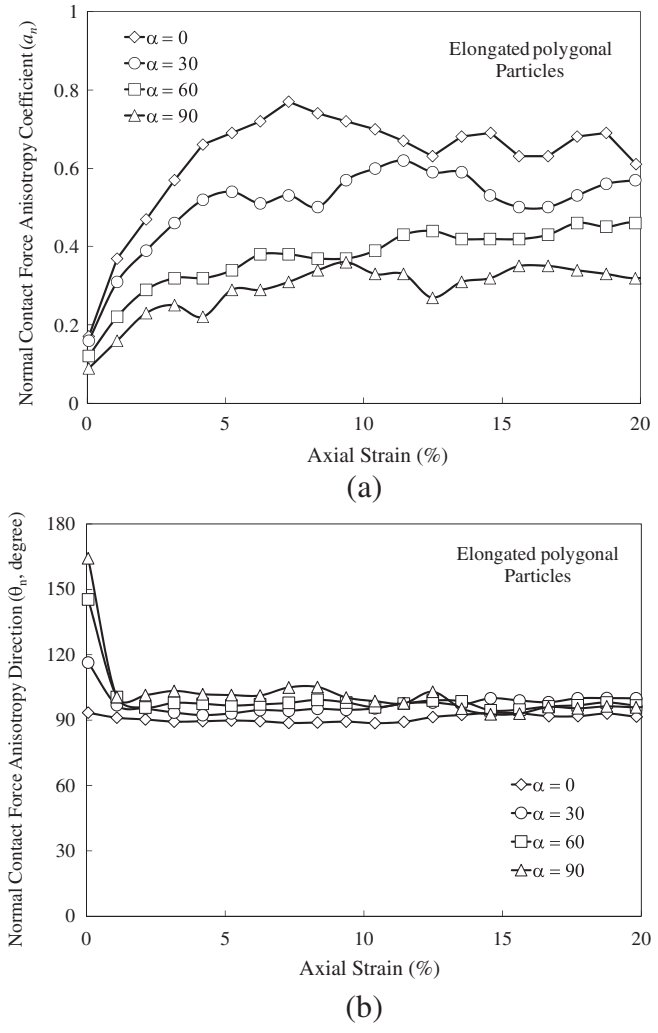

Fig. 10. Variation of normal contact force anisotropy parameters versus the axial strain for different bedding angles (a) coefficient of anisotropy; (b) principal direction of anisotropy.

deviation of contact vectors from the contact normals. When elongated particles are distributed in the medium isotropically, the average normal and tangential contact lengths are isotropically distributed too. It is noted that such isotropic condition in the fabric deviates to an induced anisotropic condition at large shear deformation as $a_{\ln}$ and a_{lt} parameters are not zero at $\varepsilon_{22} = 20\%$ anymore.

The variation of the principal directions of anisotropy of contact normal (θ_c), normal and tangential contact forces (θ_n, θ_t), and normal and tangential contact vector ($\theta_{\ln}$, θ_{lt}) is depicted in Fig. 8b. It is seen that the directions of contact normals and force components (θ_c, θ_n, θ_t) rapidly rotate to about 90°, i.e., coaxial with the principal direction of strain rate axis. The direction of contact vector components ($\theta_{\ln}$, θ_{lt}) keeps almost constant to some shear deformation and then, they abruptly rotate to about 180°. However, since their corresponding anisotropy coefficients ($a_{\ln}$, a_{lt}) are close to zero, the rotation of anisotropy direction is not significant and meaningful.

5.1.3. Inherently-anisotropic assemblies

Since the inherently-anisotropic samples considered in this study include four different bedding angles, the investigation of the anisotropy coefficients and directions are compared with each other. Fig. 9 shows the variation of the normal contact anisotropy coefficient (a_c) and the corresponding principal direction of anisotropy (θ_c) versus the axial strain. According to Fig. 9a, the initial value of the parameter a_c, which corresponds to the end of compaction process, is the same for all inherently-anisotropic samples. The non-zero and equal value for all the assemblies corresponds to the inherent anisotropy, which shows identical state of anisotropic condition for all assemblies regardless of the bedding angle. However, the variation of the contact anisotropy of each sample during the loading has a different trend depending on the bedding angle of particles. The assemblies with $\alpha = 0°$ and 30° show a growth in a_c with a higher value in $\alpha = 0_o$. In the assembly with $\alpha = 90°$, a_c starts to decrease from the onset of loading and it reaches close to zero at large axial strains ($\varepsilon_{22} = 20$ %). This falling trend indicates that the contacts tend to be distributed isotropically as the loading continues. For the assembly with $\alpha = 60°$, a_c initially decreases slightly followed by keeping a constant to the end with some fluctuations around $a_c = 0.45$. It is reminded that the growth in a_c indicates the generation of new contacts among particles along the principal direction of anisotropy and simultaneously, the contacts are lost along the perpendicular direction. The reverse phenomenon causes a reduction in a_c. The variation of major principal direction of contact anisotropy (a_c) is depicted in Fig. 9b as a function of axial strain. As a global trend, one can observe that the direction of anisotropy coincides initially with the perpendicular direction of the bedding angle, i.e., $\theta_c \approx 90° + \alpha$. However, θ_c gradually tends to rotate towards the principal strain rate axis ($\theta_c = 90°$).

The variation of normal contact force anisotropy coefficient (a_n) as a function of axial strain is plotted in Fig. 10a for all assemblies. From the onset of loading, the anisotropy in the normal contact force starts

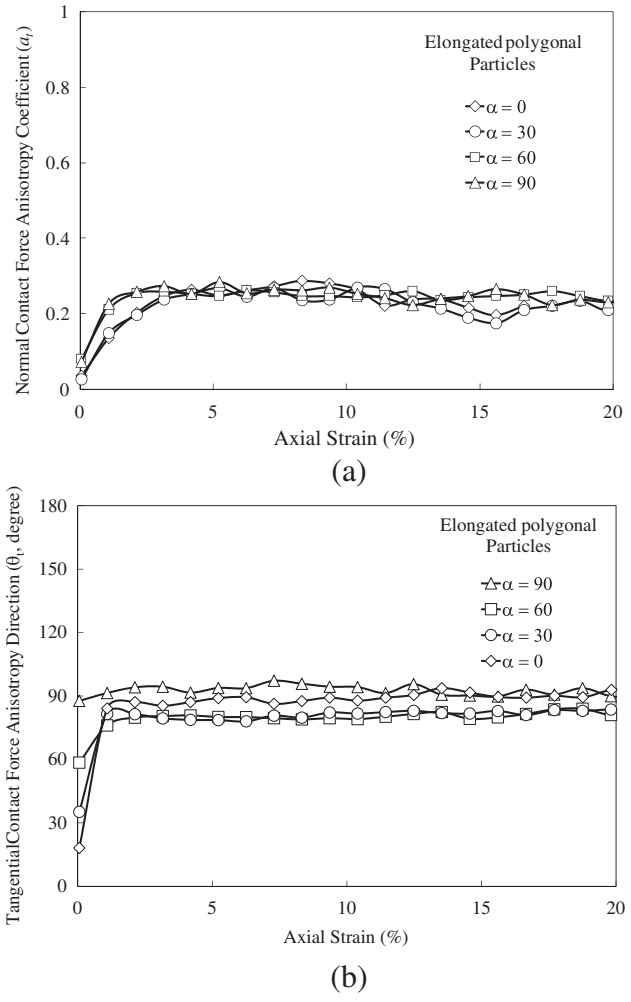

Fig. 11. Variation of tangential contact force anisotropy parameters versus the axial strain for different bedding angles (a) coefficient of anisotropy; (b) principal direction of anisotropy.

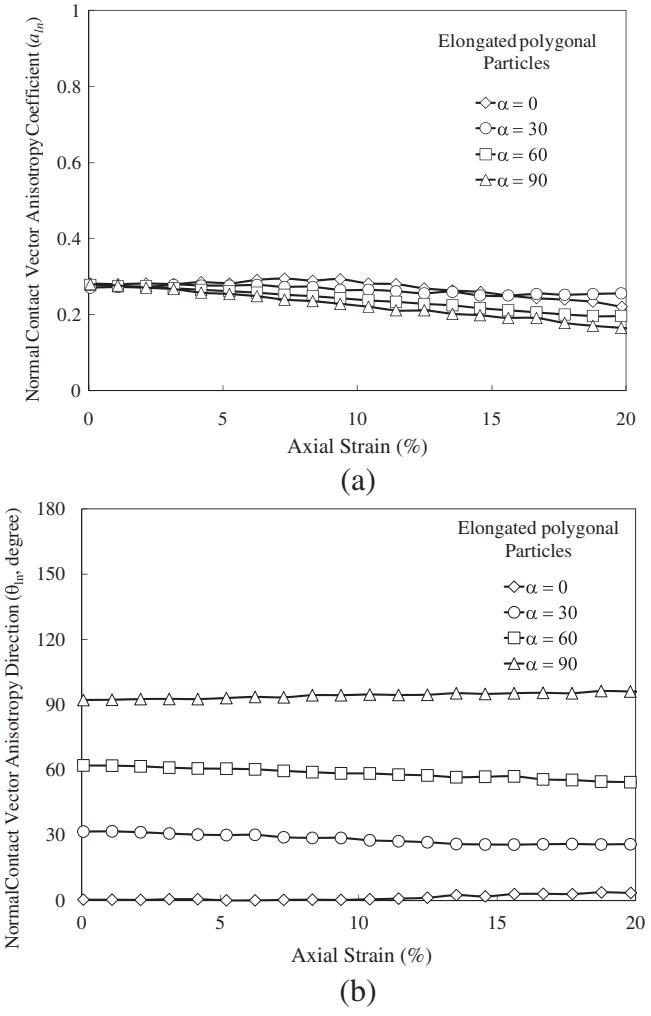

Fig. 12. Variation of normal contact vector anisotropy parameters versus the axial strain for different bedding angles (a) coefficient of anisotropy; (b) principal direction of anisotropy.

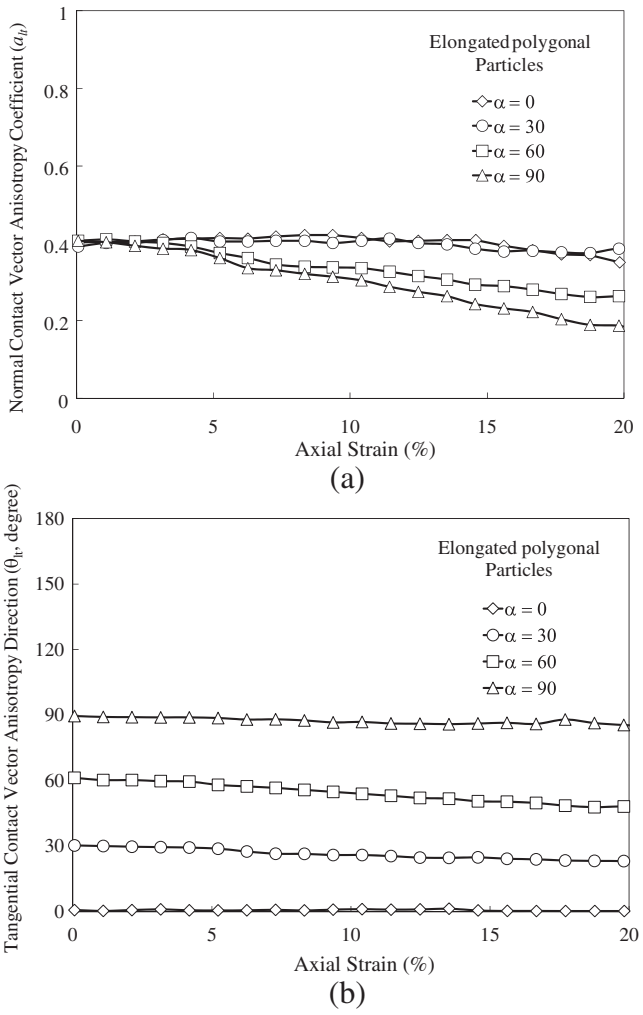

Fig. 13. Variation of tangential contact vector anisotropy parameters versus the axial strain for different bedding angles (a) coefficient of anisotropy; (b) principal direction of anisotropy.

rapidly. The mobilized value of a_n increases with the decrease of bedding angle. Fig. 10b depicts the principal direction of normal contact force anisotropy. Before the loading starts, the anisotropy direction is inclined approximately perpendicular to the bedding angle, but it rotates rapidly towards the loading axis ($\theta_n \approx 90$). Such rotation of anisotropy axis originates from the generation of new force chains along the loading axis irrespective of the arrangement of particles and in turn, the magnitude of the force chains along the horizontal direction is disintegrated [28].

According to Fig. 11a, the coefficient of tangential contact force anisotropy, a_t, shows a rapid rise to a maximum value that is followed by a very slow reduction in magnitude at large axial strain. This trend in a_t is almost the same for all the assemblies. As explained before, the mobilization of a_t corresponds to the inter-particle shear forces, which is restricted by the particles slippage. The variation in the principal orientation of the tangential contact forces, θ_t, is depicted in Fig. 11b. Analogous to what happens with the normal contact force, θ_t rotates abruptly at the initial stage of loading towards the loading axis.

Figs. 12 and 13 present the variation of anisotropy parameters versus the shear deformation for the normal (a_{ln}, θ_{ln}) and tangential (a_{ln}, θ_{ln}) components of contact vectors, respectively. It can be seen that contact length anisotropy exists in the assemblies from the beginning and after a small rise in magnitude, they both tend to decrease slowly as the shear deformation continues. Similar to the isotropic assembly, we always have: $a_{lt} > a_{ln}$. However, the magnitude of anisotropy coefficients of the contact length component is not zero. This indicates that coaxiality between the contact vector and the contact normal, which can exist among circular or isotropically-distributed particles, does not exist at all. The variation trend in a_{ln} and a_{lt} is almost the same for all anisotropic samples. Such reduction indicates that the particles tend to rotate and that the particle inclination is in such a way that they carry applied loads. A detailed comparison of the degree of particle rotation among anisotropic assemblies is given by Seyedi Hosseininia [27]. According to Figs. 12b and 13b, the principal direction of contact vector anisotropy of both normal and tangential components remains almost constant in each sample and is equal to the bedding angle (α). This is due to the elongation of particles which is oriented towards their bedding angle.

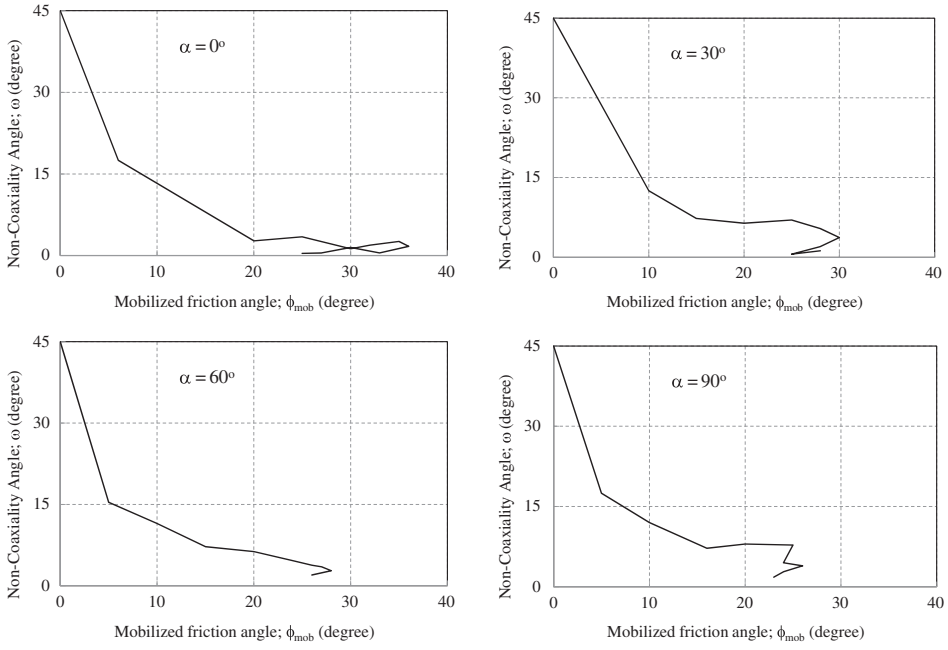

Fig. 14. Variation of non-coaxiality angle (ω) with the mobilized friction angle (ϕ_{mob}) during the tests for anisotropic assemblies.

5.2. Comparison of macro- and micro-expressions of principal stress axis rotation

The stress tensor components, i.e., σ_{11}, σ_{22}, and σ_{12} of the assemblies were measured during the loading process and thus, the non-coaxiality angle (from macro parameters) can be measured directly from Eqs. (5) and (7). The variation of non-coaxiality angle (ω) with the mobilized friction angle (ϕ_{mob}) is depicted in Fig. 14 for all anisotropic assembles. ϕ_{mob} can be calculated from the so called Mohr–Coulomb failure criterion defined as follows:

$$\phi_{mob} = \sin^{-1}\left(\frac{\sqrt{(\sigma_{11}-\sigma_{22})^2+4\sigma_{12}^2}}{\sigma_{11}+\sigma_{22}}\right). \quad (9)$$

There is the same trend in the variation of ω in terms of ϕ_{mob} for all anisotropic assemblies. As shown, the variation of ϕ_{mob} occurs at two stages including the mobilization of ϕ_{mob} to the maximum value (peak shear strength) followed by a reduction to the end of the test. The non-coaxiality angle (ω) ever decreases during the test regardless of the variation in ϕ_{mob}. ω continues to diminish towards small value close to zero even after the sample shows softening behavior.

Now, macro- and micro-expressions of principal stress axis rotation are investigated. The variation of the principal direction of stress rotation during the tests can be assessed directly by using Eq. (6). On the other hand, by having the simultaneous magnitudes of all micromechanical parameters, stress axis rotation can be calculated from a micromechanical point of view by using Eq. (7). The results from these equations are shown in Fig. 15 in terms of non-coaxiality

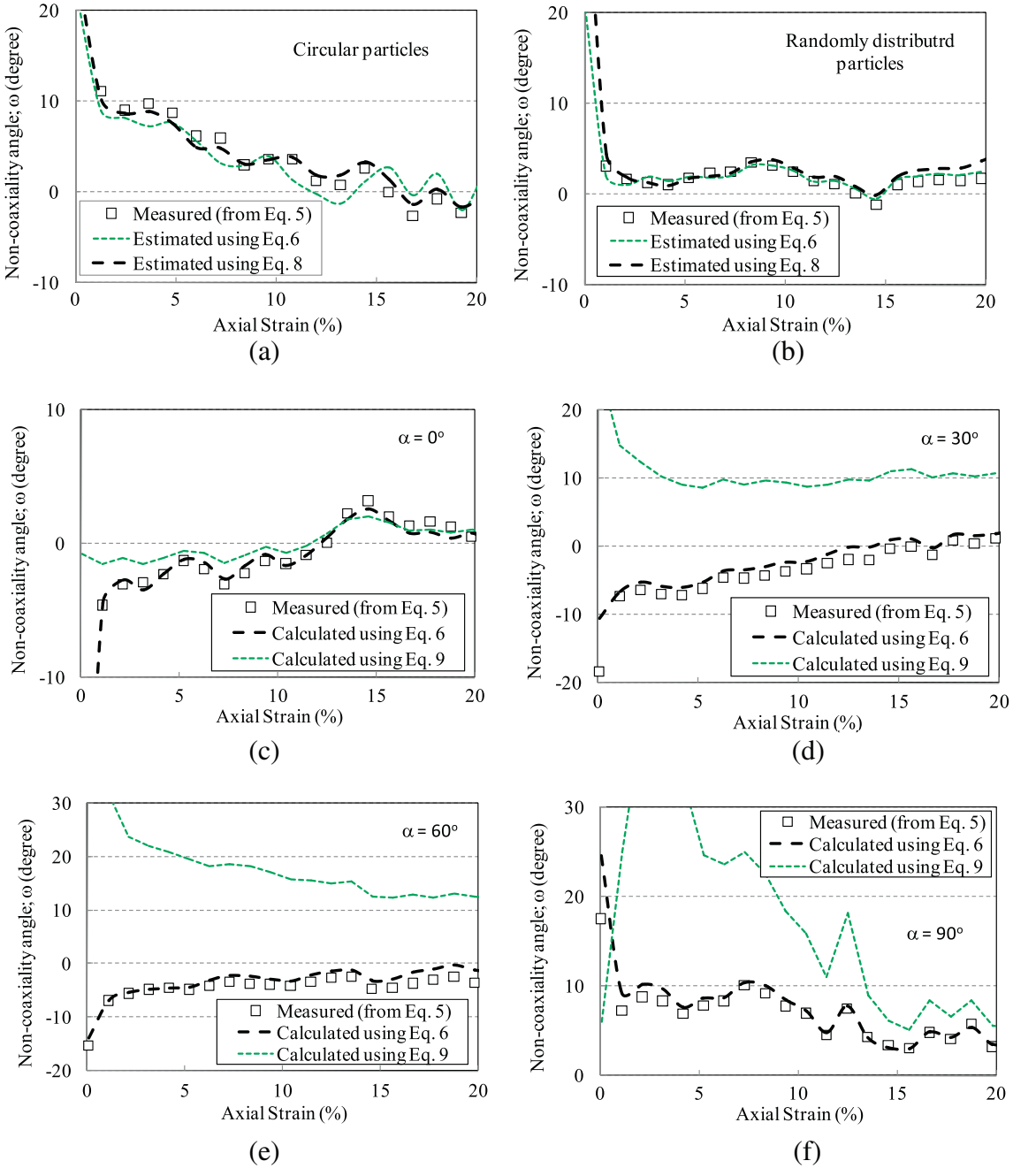

Fig. 15. Variation of non-coaxiality angles versus the axial strain for different assemblies.

angle (ω) versus the axial strain for the assemblies of circular and angular particles with isotropic and inherently-anisotropic (α = 0, 30, 60, and 90°) fabrics. As can be observed, the predicted values form the micromechanical expression which coincides well with direct measured data.

The micromechanics-based equation of the principal stress direction (Eq. (7)) can be expressed in a simpler form in the case of the granular materials with circular or randomly-distributed elongated particles. For circular particles, since the micromechanical parameters of contact vector lengths (a_{ln}, a_{lt}, θ_{ln}, θ_{lt}) are zero, the corresponding terms in the fraction of Eq. (7) are omitted. For the sample with elongated particles, the directions θ_{ln}, θ_{lt} are not zero; however, the anisotropy coefficients (a_{ln}, a_{lt}) have very small values close to zero and hence, the corresponding terms can be ignored. By paying attention to the variation of principal direction of anisotropy (Figs. 7b and 8b), we have $\theta_c \approx \theta_n \approx \theta_t$ for both the assemblies of circular and elongated particles. Accordingly, by referring back to Eq. (7) and simplifying the fraction by putting an average value of these principal anisotropy directions, $\overline{\theta} = (\theta_c + \theta_n + \theta_t)/3$, one can re-express Eq. (7) as follows:

$$\theta_\sigma^{micro} = \frac{1}{2}\tan^{-1}\left(\frac{(a_c + a_n + a_t)}{(a_c + a_n + a_t)}\tan(2\overline{\theta})\right) = \overline{\theta} \tag{10}$$

which means that the principal direction of stress axis is coincident with the average direction of anisotropy parameters of the fabric. In such case, the intensity of the fabric anisotropy (anisotropy coefficients) does not influence the rotation of stress axis at all. The predictions from Eq. (10) are depicted alongside the measured data in Fig. 15a and b. It can be seen that the simplified relationship can well estimate the observed trend in the tests.

For aggregates with inherently-anisotropic fabrics, consideration of anisotropic parameters of contact vector components in the stress–force–fabric (SFF) relationship (Eq. (1)) is essential in order to accurately predict the macroscopic behavior from micromechanical equations. If the relating contact vector anisotropic parameters are ignored, a simpler equation is obtained for the principal direction of stress axis:

$$\theta_\sigma^{micro} = \frac{1}{2}\tan^{-1}\left(\frac{a_c\sin 2\theta_c + a_n\sin 2\theta_n + a_t\sin 2\theta_t}{a_c\cos 2\theta_c + a_n\cos 2\theta_n + a_t\cos 2\theta_t}\right). \tag{11}$$

The non-coaxiality angle using the above equation is calculated for inherently-anisotropic samples and the variation is compared with the measured values in Fig. 15c trough f. As shown, the truncated equation (Eq. (11)) is not capable of predicting the rotation of stress axis at all. In other words, the participation of the terms aln and alt is not negligible. Hence, it can be concluded that in addition to contact normals and contact force components, contact vectors in a decomposed form should be also considered in the micromechanical formulations.

6. Conclusions

In this study, the rotation of principal direction of stress axis was studied from the micromechanical point of view. It is evident that the fabric evolution in a granular material is responsible for the observed behavior of the medium. Based on the general form of stress–force–fabric relationship for a granular material, a mathematical expression was derived for the direction of principal stress axis as a function of micromechanical parameters of the fabric. The fabric parameters include anisotropy coefficients as well as corresponding principal directions of normal contacts, force contact components, and contact vector components. In order to verify the macro–micro relationship, DEM was used to simulate biaxial compression tests. In these tests, circular and elongated angular particles were considered. In the simulations, the stress rotation is measured during continuous shearing at fixed strain direction. It was shown that the principal directions of anisotropy parameters including contacts and contact forces are coaxial for the assemblies containing either circular particles or elongated particles which are randomly-distributed in the medium. On the other hand, owing to the fabric condition and the particle arrangement, the contact vector distribution has an isotropic condition. As a consequence, the contact vector does not have influence on the direction of stress axis. In such case, the direction of stress axis can be regarded as the average of anisotropy directions. For the assemblies with inherently-anisotropic fabrics, however, this is not true because the contact vectors generated between contacting particles tend generally to incline towards the bedding angle and hence, an anisotropic condition arises in the fabric. Accordingly, the principal direction of stress axis is diverted from the average direction of anisotropy. In such case, it is inevitable to consider the anisotropy parameters of contact vectors in the formulation in order to accurately predict the rotation of principal stress axis.

The findings from the present study also match with the results of numerical modeling of granular media behavior in the domain of continuum. With shear loading applied on the granular medium, the fabric is persuaded to evolve and become more co-axial with the loading/stress direction and the fabric terms will gradually become coaxial with the principal stress direction, which leads to a final coaxial material response [e.g., 49]. The present work may serve a further micromechanical confirmation of these studies under rotational shear loading condition.

It is also reminded that the loading condition used in this study was a special case in such a way that the principal strain direction was fixed and the principal direction of stress was rotated and hence, the non-coaxiality could be measured. Although the formulations derived from micromechanical investigations are state-independent as well as loading-independent, extra simulations are needed in order to generalize and verify these findings for undrained condition as well as different stress paths.

Acknowledgment

The author would like to express his gratitude towards the Research Deputy of Ferdowsi University of Mashhad for supporting this project by grant No.: 26990-18/4/92. Furthermore, the author would like to thank all the reviewers for studying carefully the manuscript and enriching the paper by their valuable comments.

Appendix A. Derivation of the mathematical form of stress tensor components

According to Eq. (1), the extended mathematical form of stress normal components can be expressed as follows:

$$\begin{aligned}\sigma_{11} = m_v\int_0^{2\pi}\Big\{&\overline{f}_n(\theta)\overline{l}_n(\theta)\cos^2\theta - \left[\overline{f}_n(\theta)\overline{l}_t(\theta) + \overline{f}_t(\theta)\overline{l}_n(\theta)\right]\sin\theta\cos\theta \\ &+ \overline{f}_t(\theta)\overline{l}_t(\theta)\sin^2\theta\Big\}E(\theta)d\theta \\ \sigma_{22} = m_v\int_0^{2\pi}\Big\{&\overline{f}_n(\theta)\overline{l}_n(\theta)\sin^2\theta + \left[\overline{f}_n(\theta)\overline{l}_t(\theta) + \overline{f}_t(\theta)\overline{l}_n(\theta)\right]\sin\theta\cos\theta \\ &+ \overline{f}_t(\theta)\overline{l}_t(\theta)\cos^2\theta\Big\}E(\theta)d\theta.\end{aligned} \tag{1A}$$

Hence, we have:

$$\begin{aligned}\sigma_{11} - \sigma_{22} = m_v\int_0^{2\pi}\Big\{&\left[\overline{f}_n(\theta)\overline{l}_n(\theta) - \overline{f}_t(\theta)\overline{l}_t(\theta)\right]\cos 2\theta \\ &- \left[\overline{f}_n(\theta)\overline{l}_t(\theta) + \overline{f}_t(\theta)\overline{l}_n(\theta)\right]\sin 2\theta\Big\}E(\theta)d\theta.\end{aligned} \tag{2A}$$

By ignoring the product of anisotropy coefficients for the third and higher orders, the integration of the above expression gives:

$$\begin{aligned}\sigma_{11}-\sigma_{22} &= m_v\{a_c(2\cos^2\theta_c-1)+a_n(2\cos^2\theta_n-1)+a_t(2\cos^2\theta_t-1)\\ &\quad +a_{\ln}(2\cos^2\theta_{\ln}-1)+a_{lt}(2\cos^2\theta_{lt}-1)\}\\ &= m_v\{a_c\cos2\theta_c+a_n\cos2\theta_n+a_t\cos2\theta_t+a_{\ln}\cos2\theta_{\ln}+a_{lt}\cos2\theta_{lt}\}.\end{aligned} \tag{3A}$$

Similarly, on the other hand, for the shear component of the stress tensor, we have:

$$\begin{aligned}\sigma_{12} &= m_v\int_0^{2\pi}\left\{\begin{array}{l}\overline{f}_n(\theta)\overline{l}_n(\theta)\cos\theta\sin\theta+\overline{f}_n(\theta)\overline{l}_t(\theta)\cos^2\theta-\overline{f}_t(\theta)\overline{l}_n(\theta)\sin^2\theta\\ -\overline{f}_t(\theta)\overline{l}_t(\theta)\sin\theta\cos\theta\end{array}\right\}E(\theta)d\theta\\ &= \frac{m_v}{2}\{a_c\sin2\theta_c+a_n\sin2\theta_n+a_t\sin2\theta_t+a_{\ln}\sin2\theta_{\ln}+a_{lt}\sin2\theta_{lt}\}.\end{aligned}$$

References

[1] R. Hill, The Mathematical Theory of Plasticity, Clarendon Press, Oxford, 1950.
[2] K.H. Roscoe, R.H. Bassett, E.R. Cole, Principal axes observed during sample shear of a sand, Proceeding Conference Oslo 1967, pp. 231–237.
[3] A. Drescher, G. de Josselin de Jong, Photoelastic verification of a mechanical model for the flow of a granular material, J. Mech. Phys. Solids 20 (1972) 337–351.
[4] J.R.F. Arthur, K.S. Chua, T. Dunstan, Induced anisotropy in a sand, Geotechnique 27 (1977) 13–30.
[5] R.K.S. Wong, J.R.F. Arthur, Sand shear by stresses with cyclic variation in direction, Geotechnique 2 (1986) 215–226.
[6] Y. Cai, An Experimental Study of Non-coaxial Soil Behavior Using Hollow Cylinder Testing, Civil Engineering, University of Nottingham, Nottingham, 2010.
[7] J.R.F. Arthur, S. Bekenstein, J.T. Germaine, C.C. Ladd, Stress Path Tests With Controlled Rotation of Principal Stress Directions, American Society for Testing and Materials, Philadelphia, 1981.
[8] K. Ishihara, I. Towhata, Sand response to cyclic rotation of principal stress directions as induced by wave loadings, Soils Found. 23 (1983) 105–117.
[9] S.K. Chaudhary, J. Kuwano, Anisotropic multiple yielding of dense Toyoura sand in p′-constant shear plane, Soils Found. 43 (2003) 59–69.
[10] P.V. Lade, M.M. Kirkgard, Effects of stress rotation and changes of b-values on cross-anisotropic behavior of natural, K0-consolidated soft clay, Soils Found. 40 (2000) 93–105.
[11] K. Miura, S. Miura, S. Toki, Deformation behavior of anisotropic dense sand under principal stress axes rotation, Soils Found. 26 (1986) 36–52.
[12] H. OHKAWA, J. KUWANO, T. NAKADA, S. TACHIBANA, Yielding characteristic and non-coaxiality of Toyoura sand on p′-constant shear stress plane, Soils Found. 51 (2011) 179–190.
[13] D. PRADEL, K. ISHIHARA, M. GUTIERREZ, Yielding and flow of sand under principal stress rotation, Soils Found. 30 (1990) 87–99.
[14] H.A. Joer, J. Lanier, M. Fahey, Deformation of granular materials due to rotation of principal axes, Geotechnique 48 (1998) 605–619.
[15] M. GUTIERREZ, K. Ishihara, I. Towhata, Flow theory for sand during rotation of principal stress direction, Soils Found. 31 (1991) 121–132.
[16] K. Hashiguchi, S. Tsutsumi, Shear band deformation analysis in soils by the subloading surface model with tangential stress rate effect, Int. J. Plast. 19 (2003) 1651–1677.
[17] A. Anandarajah, Y.F. Dafalias, Bounding surface plasticity, III: application to anisotropic cohesive soils, J. Eng. Mech. ASCE 112 (1986) 1292–1318.
[18] A. Lashkari, M. Latifi, A simple plasticity model for non-coaxial flow of sand, Mech. Res. Commun. 34 (2007) 191–200.
[19] X. Li, Y.F. Dafalias, Constitutive modeling of inherently anisotropic sand behavior, J. Geotech. Geoenviron. Eng. 128 (10) (2002) 868–880.
[20] M. GUTIERREZ, K. ISHIHARA, Non-coaxiality and energy dissipation in granular materials, Soils Found. 40 (2000) 49–59.
[21] M. Gutierrez, K. Ishihara, I. Towhata, Model for the deformation of sand during rotation of principal stress directions, Soils Found. 33 (1993) 105–117.
[22] K. MIURA, S. TOKI, S. MIURA, Deformation prediction for anisotropic sand during the rotation of principal stress axes, Soils Found. 26 (1986) 42–56.
[23] M. Oda, J. Konishi, S. Nemat-Nasser, Experimental micromechanical evolution of strength of granular materials: effects of particle rolling, Mech. Mater. 1 (1982) 269–283.
[24] M. Oda, S. Nemat-Nasser, J. Konishi, Stress-induced anisotropy in granular masses, Soils Found. 25 (1985) 85–97.
[25] M. Oda, H. Kazama, J. Konishi, Effects of induced anisotropy on the development of shear bands in granular materials, Mech. Mater. 28 (1998) 103–111.
[26] Z. Mahmood, K. Iwashita, Influence of inherent anisotropy on mechanical behavior of granular materials based on DEM simulations, Int. J. Numer. Anal. Methods Geomech. 34 (2010) 795–819.
[27] E. Seyedi Hosseininia, Discrete element modeling of inherently anisotropic granular assemblies with polygonal particles, Particuology 10 (2012) 542–552.
[28] E. Seyedi Hosseininia, Investigating the micromechanical evolutions within inherently anisotropic granular materials using discrete element method, Granul. Matter 14 (2012) 483–503.
[29] M. Satake, Fabric tensor in granular materials, in: P.A. Vermeer, H.J. Luger (Eds.), Deformation and Failure of Granular Materials, Balkema, Rotterdam 1982, pp. 63–68.
[30] M.R. Horne, The Behavior of An Assembly of Rotund, Rigid, Cohesionless Particles I & II, Royal Society of London, 1965. 62–97.
[31] M. Oda, Initial fabrics and their relations to mechanical properties of granular material, Soils Found. 12 (1972) 18–36.
[32] M.M. Mehrabadi, S. Nemat-Nasser, M. Oda, On statistical description of stress and fabric in granular materials, Int. J. Numer. Anal. Methods Geomech. 6 (1982) 95–108.
[33] R. Hill, Elastic properties of reinforced solids: some theoretical principles, J. Mech. Phys. Solids 11 (1963) 357–372.
[34] O.D.L. Strack, P.A. Cundall, The distinct element method as a tool for research in granular media, Report ENG 76-20711, National Science Foundation, Dep. Civil and Mining engineering, University of Minnesota, 1978.
[35] L. Rothenburg, Micromechanics of Idealized Granular Systems, Department of Civil Engineering, Carlton University, Ottawa, 1980. 332.
[36] J. Weber, Recherches concernant les contraintes intergranulaires dans les milieu pulvérulents, Bulletin de Laison Ponts et Chaussées1966.
[37] L. Rothenburg, A.P.S. Selvadurai, A micromechanical definition of the Cauchy stress tensor for particulate media, in: A.P.S. Selvadurai (Ed.), Mechanics of Structured Media, Elsevier, Amsterdam 1981, pp. 469–486.
[38] L. Rothenburg, R.J. Bathurst, Analytical study of induced anisotropy in idealized granular materials, Geotechnique 39 (1989) 601–614.
[39] L. Rothenburg, R.J. Bathurst, Micromechanical features of granular assemblies with planar elliptical particles, Geotechnique 42 (1992) 79–95.
[40] E. Seyedi Hosseininia, A.A. Mirghasemi, Numerical simulation of breakage of two-dimensional polygon-shaped particles using discrete element method, Powder Technol. 166 (2006) 100–112.
[41] A.A. Mirghasemi, L. Rothenburg, E.L. Matyas, Numerical simulations of assemblies of two-dimensional polygon-shaped particles and effects of confining pressure on shear strength, Soils Found. 37 (1997) 43–52.
[42] X. Li, H. Yu, Particle-scale insight into deformation noncoaxiality of granular materials, Int. J. Geomech (2013)http://dx.doi.org/10.1061/(ASCE)GM.1943-5622.0000338 (04014061).
[43] E. Seyedi Hosseininia, Stress–force–fabric relationship for planar granular materials, Geotechnique 63 (2013) 830–841.
[44] F. Alonso-Marroquin, S. Luding, H.J. Herrmann, I. Vardoulakis, Role of anisotropy in the elastoplastic response of a polygonal packing, Phys. Rev. E71 (2005) 051304.
[45] C. Thronton, L. Zhang, A numerical examination of shear banding and simple shear non-coaxial flow rules, Philos. Mag. (2005) 3425–3452.
[46] K.H. Roscoe, The influence of strains in soil mechanics, Geotechnique 20 (1970) 129–170.
[47] Y. Cai, H.S. Yu, D. Wanatowski, X. Li, Noncoaxial behavior of sand under various stress paths, J. Geotech. Geoenviron. 139 (2013) 1381–1395.
[48] X. Li, H.S. Yu, Applicability of stress–force–fabric relationship for non-proportional loading, Comput. Struct. 89 (2011) 1094–1102.
[49] Z.W. Gao, J.D. Zhao, X.S. Li, Y.F. Dafalias, A critical state sand plasticity model accounting for fabric evolution, Int. J. Numer. Anal. Methods Geomech. 38 (2014) 370–390.
[50] J.D. Zhao, N. Guo, Unique critical state characteristics in granular media considering fabric anisotropy, Geotechnique 63 (2013) 695–704.
[51] A. Lashkari, M. Latifi, A simple plasticity model for prediction of non-coaxial flow of sand, Mech. Res. Commun. 34 (2007) 191–200.
[52] A. Lashkari, M. Latifi, A non-coaxial constitutive model for sand deformation under rotation of principal stress axes, Int. J. Numer. Anal. Methods Geomech. 32 (2008) 1051–1086.
[53] X.S. Li, Y.F. Dafalias, A constitutive framework for anisotropic sand including non-proportional loading, Geotechnique 54 (2004) 41–55.
[54] J.P. Bardet, I. Vardoulakis, The asymmetry of stress in granular media, Int. J. Solids Struct. 38 (2001) 53–367.
[55] R.J. Bathurst, A Study of Stress and Anisotropy in Idealized Granular Assemblies, Department of Civil Engineering, Queen's University, Kingston, 1985.
[56] T.G. Sitharam, S.V. Dinesh, N. Shimizu, Micromechanical modelling of monotonic drained and undrained shear behaviour of granular media using three dimensional DEM, Int. J. Numer. Anal. Methods Geomech. 26 (2002) 1167–1189.
[57] N. Guo, J.D. Zhao, The signature of shear-induced anisotropy in granular media, Comput. Geotech. 47 (2013) 1–15.
[58] E.T. Bowman, K. Soga, W. Drummond, Particle shape characterization using fourier descriptor analysis, Geotechnique 51 (2011) 545–554.
[59] I. Houlubec, E. D'Appolonia, Effect of particle shape on the engineering properties of granular soils, Proceedings of Symposium on Evaluation of Relative Density Los Angeles 1973, pp. 304–318.
[60] H.M. Shodjaa, E.G. Nezami, A micromechanical study of rolling and sliding contacts in assemblies of oval granules, Int. J. Numer. Anal. Methods Geomech. 27 (2003) 403–424.
[61] A.A. Peña, S. McNamara, P.G. Lind, H.J. Herrmann, Avalanches in anisotropic sheared granular media, Granul. Matter 11 (2009) 243–252.
[62] S.P. Pudasaini, K. Hutter, Avalanche Dynamics: Dynamics of Rapid Flows of Dense Granular Avalanches, Springer, Berlin, New York, 2007..